

Lattice vibrations of α' - NaV_2O_5

M. N. Popova, A. B. Sushkov, S. A. Golubchik, B. N. Mavrin, and V. N. Denisov
Institute of Spectroscopy, Russian Academy of Sciences,
142092 Troitsk, Moscow reg., Russia

B. Z. Malkin and A. I. Iskhakova
Kazan State University, 420008 Kazan, Russia

M. Isobe and Y. Ueda
Institute for Solid State Physics, The University of Tokyo
7-22-1 Roppongi, Minato-ku, Tokyo 106, Japan
 (August 19, 2019)

We have measured far infrared reflectance and transmittance spectra as well as Raman scattering spectra of α' - NaV_2O_5 single crystals for all the principal polarizations. The temperature range above the phase transition temperature $T_c = 35$ K was investigated, mainly. On the basis of this experimental study and of the lattice dynamics calculations we conclude that the symmetry of NaV_2O_5 in the high temperature phase is described by the centrosymmetric D_{2h}^{13} space group. The assignment of the observed phonons is given. Values of dielectric constants are obtained from the infrared data. Asymmetric shapes of several infrared lines as well as higher order infrared vibrational spectra are discussed. The crystal field energy levels of the $3d$ electron localized at the V^{4+} site have been calculated in the framework of the exchange charge model using the values of effective charges obtained from the lattice dynamics calculations. According to the results of these calculations, the earlier observed broad optical bands in the region of 1 eV can be interpreted as phonon assisted $d-d$ transitions.

63.20.Dj 78.30.Hv

I. INTRODUCTION

The vanadate α' - NaV_2O_5 has attracted a considerable interest recently as the second inorganic compound undergoing the spin-Peierls transition (at the highest known temperature for the spin-Peierls compounds, $T_c = 35$ K [1]). The spin-Peierls transition is expected to occur within a system of linear spin-1/2 Heisenberg antiferromagnetic chains coupled to a three-dimensional phonon field. As a result of such a coupling, magnetic atoms of the chain dimerize and a spin gap opens [2]. One-dimensional magnetic properties of NaV_2O_5 above 35 K follow from magnetic susceptibility [1], ESR [3] and angle-resolved photoemission [4] measurements.

Below 35 K the lattice dimerizes, as observed by X-ray [5] and Raman [6,7] scattering, infrared transmission [8] and reflection [9] measurements, while the magnetic susceptibility decreases isotropically, thus showing a spin gap formation [6]. The size of the gap $\Delta = 10$ meV follows from inelastic neutron scattering study of NaV_2O_5 single crystals [5,10].

The structure of NaV_2O_5 contains double chains of edge sharing distorted VO_5 pyramids running along the orthorhombic b -axis (see Fig. 1). These double chains are linked together via common corners of the pyramids to form the ab -layers. Na atoms lie between the layers [11,1]. The structure of NaV_2O_5 looks like the structure of V_2O_5 [12] intercalated with sodium. In an early X-ray room temperature investigation on polycrystalline samples of NaV_2O_5 Carpy and Galy [11] suggested the noncentrosymmetric space group $C_{2v}^7-P2_1mn$ with two nonequivalent vanadium positions in the unit cell. The picture of magnetic chains of V^{4+}O_5 ($S = 1/2$) pyramids isolated by nonmagnetic chains of V^{5+}O_5 ($S = 0$) pyramids proposed to account for one-dimensional magnetic properties of this mixed valence ($\text{V}^{4.5+}$) compound is compatible with this space group [1].

However, the recent redetermination of the structure by single crystal X-ray diffraction at room temperature was in favor of the centrosymmetric $D_{2h}^{13}-Pm\bar{m}n$ group with only one vanadium position in the structure [13,14]. Though the topology of the structure remains essentially the same as in the previously proposed noncentrosymmetric space group [11], the possibility for charge ordering is, however, lost in the new higher symmetry group. Smolinski et al. [13] and Horsch and Mack [15] suggested a quarter-filled ladder model for NaV_2O_5 , with the spins carried by V-O-V molecular orbitals on the rungs of the ladder. They argued that the exchange interaction along the ladder is much greater than that between the neighboring ladders which would explain the one-dimensional magnetic properties of the high temperature phase of NaV_2O_5 . The transition at 35 K was supposed to be an ordinary spin-Peierls transition.

Quite recent ^{51}V -NMR experiment on a single-crystalline sample of NaV_2O_5 also revealed only one vanadium position in the high temperature phase but pointed unambiguously to the existence of two different vanadium sites occupied by V^{4+} and V^{5+} at liquid helium temperatures [16]. Thus, the transition at 35 K is connected with a structure and a charge ordering processes. Very recently, Seo and Fukuyama [17] and Mostovoy and Khomskii [18] proposed a zig-zag scheme of V^{4+} - V^{5+} ordering. Seo and Fukuyama argued that, as a result, two-dimensional lattice of antiferromagnetic dimers is formed [17], while Mostovoy and Khomskii gave reasons in support of a system of alternating chains [18]. Thalmeier and Fulde [19] have presented some theoretical reasons for the primary charge ordering which provides neighboring linear V^{4+} and V^{5+} chains with the subsequent spin-Peierls transition. Two close transitions near 35 K in NaV_2O_5 were detected by Köppen et al. by the thermal expansion measurements [20].

In view of these recent works, the symmetry problem of the high temperature phase seems to be a matter of great urgency. Raman and infrared measurements could give an additional information to clarify the question whether the space group is centrosymmetric or not, because of totally different selection rules in these two cases. We reanalyzed our earlier infrared and Raman spectra of NaV_2O_5 [21] and found that they are in a better agreement with the centrosymmetric D_{2h}^{13} space group than with the noncentrosymmetric C_{2v}^7 one. However, in our work [21] we did not measure infrared spectra in the $\mathbf{E}||\mathbf{c}$ polarization. Also, the signal-to-noise ratio of Raman spectra was rather low. In the present work, we reinvestigate vibrational spectra of the high temperature phase of NaV_2O_5 using different single crystals, including extraordinary big ones. We present far-infrared reflectivity as well as Raman-scattering spectra for all principal polarizations. In addition, transmittance spectra were studied. We show that our results are in a much better agreement with the centrosymmetric D_{2h}^{13} group than with the noncentrosymmetric C_{2v}^7 one. The assignment of vibrational modes is given based on a comparison with results on the previously studied V_2O_5 [22] and on lattice dynamics calculations of this work performed in the framework of the rigid ion model.

II. EXPERIMENTAL

Single crystals of stoichiometric α' - NaV_2O_5 used in this study were grown by a melt growth method using NaVO_3 as a flux [23]. Samples from different batches were used. One sample was $1.3 \times 8 \times 1$ mm, another one was $3 \times 17.3 \times 1.6$ mm along a -, b - and c -axes, respectively. For transmission measurements we have prepared four thin samples cleaved perpendicular to the c -axis. Their thicknesses were 110 ± 1 , 45 ± 5 , 14 ± 1.5 and 6 ± 1 μm . The samples were checked with X-ray diffraction, magnetization and ESR measurements. They exhibited a sharp transition at about 35 K.

Reflection and transmission measurements were performed with a BOMEM DA3.002 Fourier-transform spectrometer at nearly normal incidence of polarized infrared radiation. The following geometries of the experiment were used: 1) $\mathbf{k}||\mathbf{c}$, $\mathbf{E}||\mathbf{a}$ and $\mathbf{E}||\mathbf{b}$; 2) $\mathbf{k}||\mathbf{a}$, $\mathbf{E}||\mathbf{c}$ and $\mathbf{E}||\mathbf{b}$. Room temperature reflectance and transmittance spectra were measured in a spectral range 30–5000 cm^{-1} with a resolution 0.5–2.0 cm^{-1} . Using both reflectance and transmittance spectra, the absorption coefficient α was calculated. Low temperature (down to 6 K) transmittance spectra were measured with a He vapor cryostat in the spectral range 30–1000 cm^{-1} with a resolution 0.05–1.0 cm^{-1} .

Raman spectra were excited at room temperature by the 514 nm and 488 nm lines of an Ar-ion laser in backscattering geometries, dispersed by a home-made triple spectrograph and recorded using a multichannel system consisting of an image intensifier tube with a multichannel plate and a vidicon.

III. RESULTS

A. Factor-group analysis

There are two formula units and, hence, 16 atoms in the NaV_2O_5 orthorhombic unit cell with lattice constants $a = 1.1316$ nm, $b = 0.3611$ nm, $c = 0.4797$ nm [11,13,14]. Below, we present the results of factor-group analysis for both centrosymmetric D_{2h}^{13} [13,14] and noncentrosymmetric C_{2v}^7 [11] space groups.

a. Space group D_{2h}^{13} - $Pm\bar{m}n$ The notation $Pm\bar{m}n$ refers to the standard setting, such that $x||a$, $y||b$, $z||c$. It follows from X-ray diffraction data of Refs. [13,14] that Na atoms occupy $2b$ positions (the corresponding fractional atomic coordinates are defined by the basis vectors $\mathbf{r}_1(\text{Na}) = -\mathbf{r}_2(\text{Na}) = (1/4, -1/4, z_1)$, $z_1 = 0.8592$) and oxygen O1 atoms occupy $2a$ positions ($\mathbf{r}_1(\text{O1}) = -\mathbf{r}_2(\text{O1}) = (1/4, 1/4, z_2)$, $z_2 = 0.5195$), both these positions having C_{2v}^z local symmetry. V, O2 and O3 atoms reside in different $4f$ positions ($\mathbf{r}_1(\text{A}) = -\mathbf{r}_3(\text{A}) = (x_A, 1/4, z_A)$, $\mathbf{r}_2(\text{A}) = -\mathbf{r}_4(\text{A}) = (1/2 - x_A, 1/4, z_A)$, $x_V = 0.40212$, $z_V = 0.39219$, $x_{O2} = 0.57302$, $z_{O2} = 0.48769$, $x_{O3} = 0.38548$, $z_{O3} = 0.05803$) with the local symmetry C_s^{xz} . These positions yield the following irreducible representations [24,25]:

$$C_{2v}^z : \Gamma = A_g + B_{2g} + B_{3g} + B_{1u} + B_{2u} + B_{3u}$$

$$C_s^{xz} : \Gamma = 2A_g + B_{1g} + 2B_{2g} + B_{3g} + A_u + 2B_{1u} + B_{2u} + 2B_{3u}$$

Multiplying the representations given above by the number of different positions of the appropriate symmetry, summarizing them and subtracting acoustic modes ($B_{1u} + B_{2u} + B_{3u}$), we obtain the following NaV_2O_5 optical vibrational modes:

$$\begin{aligned} \Gamma_{\text{NaV}_2\text{O}_5}^{vib}(Pmmn) = & 8A_g(aa, bb, cc) + 3B_{1g}(ab) + \\ & + 8B_{2g}(ac) + 5B_{3g}(bc) + 3A_u + \\ & + 7B_{1u}(\mathbf{E}|\mathbf{c}) + 4B_{2u}(\mathbf{E}|\mathbf{b}) + 7B_{3u}(\mathbf{E}|\mathbf{a}) \end{aligned} \quad (1)$$

There are 45 vibrational modes in total. A_u modes being silent, 24 Raman ($A_g, B_{1g}, B_{2g}, B_{3g}$) and 18 infrared (B_{1u}, B_{2u}, B_{3u}) active modes are expected to be found in the spectra of NaV_2O_5 , provided the crystal space group is D_{2h}^{13} .

b. Space group C_{2v}^7 - $P2_1mn$ In their original work [11] Carpy and Galy adopted the axes setting for the $P2_1mn$ space group. Below, we use the standard setting for the $Pmn2_1$ space group: $x||b, y||c, z||a$. There are two nonequivalent V positions, five nonequivalent O positions and one Na position in this group, all of them being $2a$ positions with C_s^{yz} local symmetry. In the same way as in the previous case, using tables [25] and subtracting acoustic modes ($A_1 + B_2 + B_1$), we find the following vibrational modes:

$$\begin{aligned} \Gamma_{\text{NaV}_2\text{O}_5}^{vib}(Pmn2_1) = & 15A_1(aa, bb, cc; \mathbf{E}|\mathbf{a}) + \\ & + 8A_2(bc) + 7B_1(ab; \mathbf{E}|\mathbf{b}) + 15B_2(ac; \mathbf{E}|\mathbf{c}) \end{aligned} \quad (2)$$

There are 45 optical modes again. But in the case of this noncentrosymmetric space group all of them are Raman active, 37 of them are also infrared active.

B. Infrared spectra

Fig. 2 shows the room temperature far-infrared reflectivity spectra of NaV_2O_5 for different polarizations of the incident light. Experimental data are presented by open circles. Measured spectra were least-squares fitted by the spectra computed according to the expression

$$\mathcal{R} = \left| \frac{\sqrt{\varepsilon} - 1}{\sqrt{\varepsilon} + 1} \right|^2 \quad (3)$$

The classical dispersion formula for N independent damped oscillators was used:

$$\varepsilon = \varepsilon_\infty + \sum_{i=1}^N \frac{4\pi f_i \omega_i^2}{\omega_i^2 - \omega^2 - i\gamma_i \omega} \quad (4)$$

For $\mathbf{E}|\mathbf{b}$ and $\mathbf{E}|\mathbf{a}$ polarizations the number of oscillators and initial values of parameters were taken from the transmittance spectra ([21] and the present work). The peculiarity at 1014 cm^{-1} in $\mathbf{E}|\mathbf{a}$ polarization crossed out in Figs. 2 and 3 and observed also in $\mathbf{E}|\mathbf{b}$ polarization for some samples depends on a particular sample and is not, evidently, an intrinsic property of NaV_2O_5 . It was not taken into account in the fitting procedure. In addition to weakly damped phonon oscillators, an overdamped oscillator centered at about 300 cm^{-1} ($\omega_i = 291 \text{ cm}^{-1}$, $\gamma_i = 260 \text{ cm}^{-1}$, $f_i = 0.38$) was introduced in $\mathbf{E}|\mathbf{a}$ polarization to account for a low frequency part of a broad absorption band of a complex two-humped shape found in our previous study [21] (see also Fig 3). We failed to model the high frequency hump of this band centered at about 1000 cm^{-1} by a similar oscillator and did not try to use a more complicated model. This results in a not so good fitting of the high frequency part of the reflectance spectrum. In $\mathbf{E}|\mathbf{a}$ polarization the phonon at about 150 cm^{-1} could not be fitted well. This line is strongly asymmetric in transmittance spectra, obviously, due to the interaction with the underlying broad band.

A small bump in reflection at 939 cm^{-1} shown by the arrow in Fig 2 corresponds to the Fano-type resonance [26] well seen in the absorbance spectrum (Fig. 3). One more such a resonance becomes visible below 200 K at the frequency of about 91 cm^{-1} (see Fig. 4 and also Ref. [8]). We fitted the absorption coefficient in the vicinity of these two strongly asymmetric lines by the expression [26]:

$$\alpha(\omega) = \alpha_B(\omega) + \alpha_0 \frac{q^2 + 2\xi q - 1}{1 + \xi^2} \quad (5)$$

where $\xi = (\omega - \omega_r)/\gamma$, $\alpha_B(\omega)$ is a slowly varying broad band absorption (it is shown by a dashed line in the vicinity of the 939 cm^{-1} sharp resonance in Fig. 3), α_0 , ω_r , γ and q being variable parameters. Such an expression describes various physical situations of a sharp transitions being overlapped by a broad continuum. The lineshape of a sharp transition is changed by an interference with a continuum and depends essentially on the strength of an interaction between discrete and continuum states. The parameter q being inversely proportional to the matrix element of an interaction, the case $|q| = \infty$ corresponds to zero interaction and results in a normal Lorentzian resonance, $|q| = 1$ yields a dispersion-like curve, while $|q| = 0$ gives an inverted Lorentzian (antiresonance). The ratio α_0/α_B shows what fraction of the continuum states interacts with a sharp excited state. The results of the fitting are displayed in the inset of Fig. 3 and in Fig. 4. A similar fitting should be performed for the resonance at about 150 cm^{-1} but we failed to construct $\alpha_B(\omega)$ in this case. The parameters obtained from the fittings are listed in Table 1. ω_{TO} and γ_{TO} stand for ω_i and, correspondingly, γ_i of Eq. (4) or for ω_r and γ of Eq. (5). LO frequencies and damping constants were calculated as complex roots of the equation $\varepsilon(\omega) = 0$.

The left inset of Fig. 4 presents the temperature dependence of the Fano parameter q for the spectral line near 91 cm^{-1} for the temperatures higher than $T_c = 35 \text{ K}$. It should be mentioned that below 35 K , the shape of this line changes to an ordinary Lorentzian lineshape (see the right inset of Fig. 4 and also [8]). Simultaneously, a continuum absorption diminishes markedly in this spectral region while it practically does not change at the maximum of the low-frequency hump at 320 cm^{-1} .

With decreasing the temperature, besides the asymmetric resonance at 91 cm^{-1} in $\mathbf{E}||\mathbf{a}$ transmission, two lines at 215 and 225 cm^{-1} appear in $\mathbf{E}||\mathbf{b}$ transmittance spectra as well [8,21]. We have studied the resonances at 91 and 939 cm^{-1} ($\mathbf{E}||\mathbf{a}$); 215 and 225 cm^{-1} ($\mathbf{E}||\mathbf{b}$) for the samples of different thicknesses and found that while the intensity of 91 , 939 and 225 cm^{-1} lines grow proportionally to the sample thickness d (that is, $\alpha = \text{const}$), the intensity of the 215 cm^{-1} line does not, practically, depend on the thickness ($\alpha d \simeq \text{const}$). Consequently, while the frequencies 91 and 939 cm^{-1} ($\mathbf{E}||\mathbf{a}$) and 225 cm^{-1} ($\mathbf{E}||\mathbf{b}$) correspond to intrinsic resonances, $\omega = 215 \text{ cm}^{-1}$ must refer to a surface excitation. All the observed infrared phonon frequencies together with the calculated ones are displayed in Table 1.

NaV_2O_5 crystals are well transparent in the frequency region between 2500 and 4500 cm^{-1} and below 100 cm^{-1} . In these regions, an interference pattern was observed in ($\mathbf{E}||\mathbf{a}$) and ($\mathbf{E}||\mathbf{b}$) transmittance spectra of the samples of good quality. We also managed to observe the interference pattern below 100 cm^{-1} in $\mathbf{E}||\mathbf{c}$ transmittance of 1.3 mm thick sample. By measuring the distances Δ between the interference maxima, we have found the values of the refractive indexes n according to the relation

$$\Delta = \frac{1}{2dn}, \quad (6)$$

d being the thickness of a sample. The appropriate values of $\varepsilon = n^2$ are listed in Table 1.

We also looked for the higher order vibrational spectra by measuring the transmittance of thick ($d=0.4\text{--}3.0 \text{ mm}$) samples in the frequency range $1000\text{--}4000 \text{ cm}^{-1}$. While no pronounced features were found in $\mathbf{E}||\mathbf{a}$ and $\mathbf{E}||\mathbf{b}$ polarizations, sharp resonances were observed in $\mathbf{E}||\mathbf{c}$ ($\mathbf{k}||\mathbf{a}$) polarization at 1930 , 2858 and, possibly, 1072 and 1270 cm^{-1} , the latter two lines being somewhat masked by the edge of a strong phonon at 955 cm^{-1} (see Fig. 5).

C. Raman spectra

Polarized room-temperature Raman spectra of NaV_2O_5 in the spectral range $80\text{--}1000 \text{ cm}^{-1}$ are shown in Fig. 6. One can see immediately that the three diagonal components aa , bb , cc of the Raman scattering tensor differ markedly one from another which points to a considerable anisotropy of the structure. The most intense spectra were observed in the A_g geometry $a(cc)\bar{a}$. The intensity of the lines marked by asterisks in $B_{ig}(i = 1, 2, 3)$ spectra depended strongly on slight variations in the sample orientation. Evidently, these lines are present due to a leakage of strong lines from A_g geometries. We failed to assign for certain a weak feature near 100 cm^{-1} in the $b(ac)\bar{b}$ spectrum overlapped by a strong unshifted line present in this geometry. Possibly, it comes from a leakage of a very strong line 90 cm^{-1} from the (cc) polarization. Frequencies of the observed Raman modes together with the calculated ones are collected in Table 2.

As we have already communicated [21], besides relatively narrow lines, a broad band with a maximum near 600 cm^{-1} is observed in the $c(aa)\bar{c}$ spectrum (see Fig. 6). Since this band appears under both 514.5 nm and 488 nm excitation, we conclude that it originates from the Raman scattering process. However, a big width of this band (213 cm^{-1}), practically independent of the temperature, does not permit to assign it to fundamental modes.

We have also studied Raman spectra of Na-deficient samples $\text{Na}_{1-x}\text{V}_2\text{O}_5$ ($x = 0, 0.05, 0.10, 0.15$). The most prominent changes occur in the A_g (aa) spectrum (see Fig. 7). The 447 cm^{-1} Raman line moves to higher frequencies with growing x . Its position shown by the vertical dashed lines in Fig. 7 is 477 cm^{-1} for the sample with $x = 0.15$.

The maximum of the broad band moves in the opposite direction, namely, from 632 cm⁻¹ for $x = 0$ to 562 cm⁻¹ for $x = 0.15$. Such a change of the frequency difference between these two Raman bands is caused, probably, by a change of intermode interaction. The shape of the broad band can be approximated well by a Gaussian for all the values of x , its width growing from 213 cm⁻¹ for $x = 0$ to 290 cm⁻¹ for $x = 0.15$. As for phonon Raman lines, their shape is almost Lorentzian, their width grows too. For example, the lines 177, 301 and 531 cm⁻¹ broaden from, correspondingly, 11, 18 and 20 cm⁻¹ for $x = 0$ to 16, 27 and 34 cm⁻¹ for $x = 0.15$. The broadening of Raman bands with growing x is, evidently, connected with an increase of lattice disorder.

It is difficult to compare absolute intensities of the spectra for different x . However, certain conclusions concerning the relative intensities in a given spectrum can be drawn. The most prominent features are the growth of the intensity of the 301 cm⁻¹ line and the appearance of a new line at 988 cm⁻¹ for $x = 0.15$. All these results were obtained by decomposing of the observed spectrum into separate spectral contours. An example of such a decomposition is shown in Fig. 8.

D. Calculations of vibrational spectra

To obtain an information about the phonon spectrum of NaV₂O₅ throughout the Brillouin zone which is necessary for the analysis of the spin-phonon interaction effects, we have considered the lattice dynamics of this crystal in the framework of the rigid ion model. The goal of this study is to display the basic pairwise interion interactions which determine the main features of the measured Raman and infrared transmittance and reflectance spectra.

From the measured large TO–LO splittings of some normal modes at the Brillouin zone center (Γ point), it is clear that long-range Coulomb forces play an essential role in the formation of the vibrational spectrum of NaV₂O₅. The potential energy of the lattice was represented by a sum of Coulomb and non-Coulomb interactions. The Coulomb terms in the dynamical matrix were calculated exactly by using the Ewald method. Non-Coulomb interactions in the form of the Born-Mayer potentials with the exponential dependence on the interionic distance r ($\varphi_{ij}(r) = A_{ij} \exp(-r/\rho_{ij})$) were introduced between V–O (five bonds per vanadium ion), Na–O (eight bonds per sodium ion) and O–O neighboring ions at interionic distances shorter than 0.325 nm. Because of the nonequivalence of the oxygen O1, O2 and O3 ions we should introduce different potentials for different types of bonding. At the initial step we confined ourselves by only 10 fitting parameters (instead of 34 independent force constants for the V₂O₅ lattice in Ref. [22]) including ion charges $Z(A)$ (a condition of the lattice neutrality brings the relation $Z(\text{Na}) + Z(\text{O1}) + 2Z(\text{V}) + 2Z(\text{O2}) + 2Z(\text{O3}) = 0$ about) and A_{ij} , ρ_{ij} constants for V–O, Na–O and O–O pairs of ions.

The theoretical analysis of the vibrational spectra has been carried out for both proposed in the literature lattice structures. We did not obtain any physically well-grounded set of parameters which might provide the stable C_{2v}^7 lattice structure. So, we discuss further in this section only vibrations of the centrosymmetric lattice with the D_{2h}^{13} space group.

The orthogonal transformation of the atomic displacements to the symmetrized and normalized linear combinations, namely,

$$\begin{aligned} u_\alpha(\Gamma_{1u}, A) &= (u_{1\alpha}(A) + u_{2\alpha}(A) + u_{3\alpha}(A) + u_{4\alpha}(A))/2, \\ u_\alpha(\Gamma_{1g}, A) &= (-u_{1\alpha}(A) - u_{2\alpha}(A) + u_{3\alpha}(A) + u_{4\alpha}(A))/2, \\ u_\alpha(\Gamma_{2u}, A) &= (-u_{1\alpha}(A) + u_{2\alpha}(A) - u_{3\alpha}(A) + u_{4\alpha}(A))/2, \\ u_\alpha(\Gamma_{2g}, A) &= (u_{1\alpha}(A) - u_{2\alpha}(A) - u_{3\alpha}(A) + u_{4\alpha}(A))/2, \\ u_\alpha(\Gamma_{1u}, B) &= (u_{1\alpha}(B) + u_{2\alpha}(B))/\sqrt{2}, \\ u_\alpha(\Gamma_{1g}, B) &= (-u_{1\alpha}(B) + u_{2\alpha}(B))/\sqrt{2}, \end{aligned}$$

where A stands for V, O2 or O3 ions, and B — for Na or O1 ions, divides the dynamical matrix at the Γ -point into blocks corresponding to the irreducible representations of the crystal factor-group. Here,

$$\begin{aligned} \text{for } \alpha = x, \Gamma_{1u} &= B_{3u}, \Gamma_{1g} = B_{2g}, \Gamma_{2u} = B_{1u}, \Gamma_{2g} = A_g, \\ \text{for } \alpha = y, \Gamma_{1u} &= B_{2u}, \Gamma_{1g} = B_{3g}, \Gamma_{2u} = A_u, \Gamma_{2g} = B_{1g}, \\ \text{for } \alpha = z, \Gamma_{1u} &= B_{1u}, \Gamma_{1g} = A_g, \Gamma_{2u} = B_{3u}, \Gamma_{2g} = B_{2g}. \end{aligned}$$

From fitting of the calculated eigenvalues of the dynamical matrix to the measured frequencies of the lattice normal modes, we obtained the following values of effective ionic charges: $Z(\text{V}) = 2.405$, $Z(\text{Na}) = 0.83$, $Z(\text{O1}) = -1.22$, $Z(\text{O2}) = -1.23$, $Z(\text{O3}) = -0.98$ in units of the proton charge. The apical oxygen ion O3 closest to the vanadium ion has the lowest charge. The average values of parameters defining the Born-Mayer potentials equal $A_{ij} = 12.2$; 0.82; 12.8 (in units of 10³ eV), $\rho_{ij} = 0.0181$; 0.031 and 0.0212 nm for the V–O, Na–O and O–O bonds, respectively. It should be noted that we had to correct some force constants calculated with these potentials (the relative values of corrections are the most significant for the distant O–O bonds but do not exceed 50%) to improve a comparison between theory and experiment.

The calculated frequencies of the lattice normal modes at the Brillouin zone center are presented in Tables 1 and 2 for infrared and, correspondingly, Raman active modes. The calculated frequencies of silent A_u modes equal 120, 167 and 572 cm^{-1} . Acoustical properties of the lattice are defined by nine elastic constants, the predicted values of $C_{11} = 17.7$, $C_{12} = 9.7$, $C_{22} = 23.6$ (in units of 10^{10} N/m^2) are less dependent on variations of the model parameters.

The measured components of the high frequency dielectric tensor ε_∞ remarkably differ from unity (see Table 1), thus a neglect of the electronic polarization is a very crude approximation in this case, in particular, when estimating LO–TO splittings in the Γ point. However, for most of the infrared active normal modes, our model gives a satisfactory description of the longitudinal macroscopic electric field induced by the vibrations of ions. A very strong damping of the B_{1u} TO mode at the frequency of 591 cm^{-1} may be the reason for a large difference between the calculated and measured LO–TO splitting (see Table 1); in the case of the B_{2u} TO mode at 365 cm^{-1} our model gives strongly overestimated frequency of the corresponding LO mode. Rather large discrepancies between several calculated frequencies of the Raman active modes and the experimental data (see Table 2) clearly demonstrate that some significant interactions, in particular, the three body forces, greatly affecting frequencies of the bending vibrations, are to be included in the more thorough study of the lattice dynamics of this system.

Maybe, the most interesting result of this analysis of the NaV_2O_5 lattice dynamics is the predicted soft mode behavior of the transverse acoustical mode at the Brillouin zone boundary (with the wave vector $\mathbf{k}_0 = \pi(0, 0, 1/c)$) polarized in the ac -plane. Due to a competition of the long range Coulomb and short range non-Coulomb forces, the corresponding branch of the vibrational spectrum moves to the range of imaginary frequencies when approaching the \mathbf{k}_0 point thus opening a possibility to consider the NaV_2O_5 crystal as an improper virtual ferroelastic. To stabilize the lattice in respect to \mathbf{k}_0 -excitations, we had to introduce an attractive interaction between the neighboring V_1 and V_2 (V_3 and V_4) ions along the a -axis with the significant bending force constant of approximately 5 N/m . The charge ordering in the subsystem of V ions can destroy a balance between the forces of different signs and induce a freezing of the soft mode atomic displacements (the unit cell doubles in the c direction, the neighboring layers shift in the opposite directions, in each layer the right and left legs of the vanadium ladders become nonequivalent due to shifts of V_1 – V_2 and V_3 – V_4 rungs along opposite directions in the ac -plane) as a precursor of the subsequent magnetic ordering with doubling of a unit cell in a -, b - and c -directions.

IV. DISCUSSION

A. Symmetry group of NaV_2O_5

Table 3 summarizes the observed vibrational modes together with their interpretation both in centrosymmetric D_{2h}^{13} and noncentrosymmetric C_{2v}^7 groups. While the former group explains naturally the experimental data provided one Raman and three infrared frequencies not being detected, the latter group leads to an assumption that 22 of 45 expected Raman and 23 of 37 expected infrared modes were not detected. Moreover, only three frequencies (90 cm^{-1} , 174 and 951 cm^{-1}) coincide within the experimental precision ($\pm 4\text{ cm}^{-1}$) in the sets of Raman and infrared modes corresponding to a given irreducible representation of the noncentrosymmetric group, while all the modes should be both Raman and infrared active in that case. We also remind once more that we failed to obtain a realistic set of force constants when carrying out the lattice dynamics calculations in the assumption of C_{2v}^7 noncentrosymmetric space group.

We consider our Raman and infrared data as well as the results of lattice dynamics calculations to support strongly the conclusion of the previous structural study [13,14] that the space group of NaV_2O_5 above $T_c = 35\text{ K}$ is the centrosymmetric D_{2h}^{13} rather than noncentrosymmetric C_{2v}^7 group. From the point of view of D_{2h}^{13} group it is also easy to explain the results of a recent ^{51}V -NMR study [16] that revealed only one vanadium position at elevated temperatures.

B. Atomic displacements

As we have already mentioned in the Introduction, the structure of NaV_2O_5 looks like the structure of V_2O_5 intercalated with Na. The V–O bond lengths within the vanadium-oxygen layers are close in these two compounds (see Table 4). The longest bond within the layer interconnects two V_2O_5 units in the crystal unit cell (see Fig. 1b where this bond is indicated as a dashed line). So, it is of a certain meaning to classify the $k = 0$ crystal vibrations on the basis of internal vibrations of the V_2O_5 “molecule” (C_{2v} point symmetry group) split into Davydov doublets of the D_{2h} factor group by an interaction between two “molecules” in the crystal unit cell. ($A_g + B_{1u}$), ($B_{2g} + B_{3u}$), ($B_{3g} + B_{2u}$) and ($B_{1g} + A_u$) Davydov doublets come from A_1 , B_1 , B_2 and, correspondingly, A_2 vibrations of the V_2O_5

“molecule”. Splittings of these doublets can be as big as 100 cm^{-1} due to Coulomb interactions and, in particular, due to interactions between the adjacent V ions through the common neighbors (O2 ions) along the chains (see Fig. 1). Many of the vibrational frequencies of $\text{Na V}_2\text{O}_5$ are close to those of V_2O_5 [22].

The comparison of our observed vibrational frequencies with those of V_2O_5 [22] and with the results of our calculations leads to the following assignment of the vibrational modes of NaV_2O_5 . The V–O3 stretching modes manifest themselves by two Davydov doublets: $951 \text{ cm}^{-1} (B_{2g}) + 939 \text{ cm}^{-1} (B_{3u})$ and $970 \text{ cm}^{-1} (A_g) + 955 \text{ cm}^{-1} (B_{1u})$. The Davydov splittings are relatively small in this case indicating that these vibrations associated with the strongest bond V–O3 are really well localized. The mode frequencies are somewhat lower than the corresponding frequencies in V_2O_5 (976, 982, 994 and 975 cm^{-1}), which is in accordance with longer V–O3 bonds in NaV_2O_5 in comparison with V_2O_5 . The following vibrations are associated with the O1–V–O3 bending modes: $177 \text{ cm}^{-1} (A_g)$, $162 \text{ cm}^{-1} (B_{1u})$, $392 \text{ cm}^{-1} (B_{2g})$, $366 \text{ cm}^{-1} (B_{3g})$.

The bridging oxygens O1 participate in the bending V–O1–V vibrations $418 \text{ cm}^{-1} (B_{3g})$, $367 \text{ cm}^{-1} (B_{2u})$, $447 \text{ cm}^{-1} (A_g)$, $468 \text{ cm}^{-1} (B_{1u})$. The stretching V–O1–V vibration is placed at $420 \text{ cm}^{-1} (A_g)$ and involves mainly the motion of the V atoms along the a -axis.

The modes at $683 \text{ cm}^{-1} (B_{3g} \text{ and } B_{1g})$ and $582 \text{ cm}^{-1} (B_{2u})$ correspond to the stretching V–O2 vibrations along the b -axis while those at $550 \text{ cm}^{-1} (B_{2g})$, $533 \text{ cm}^{-1} (A_g)$ and $526 \text{ cm}^{-1} (B_{3u})$ — to the bending ones.

Most of the remaining modes can be described in terms of external modes of the V_2O_5 units. Thus, the modes at $186 \text{ cm}^{-1} (B_{2g})$, $169 \text{ cm}^{-1} (B_{3g})$ and $90 \text{ cm}^{-1} (A_g)$, correspond to the relative translations of the two V_2O_5 units within the crystal unit cell along the a -, b - and, correspondingly, c -axes. As the V_2O_5 units are bound together along the b -axis, these modes can be considered as relative translations of the neighboring $(\text{VO}_5)_n$ chains. The B_{1g} mode at 174 cm^{-1} (O3 ions move along the b -axis) and the A_g mode at 301 cm^{-1} (O2 ions move along the c -axis) correlate with in-plane and, correspondingly, out-of-plane chain bending vibrations. The B_{2g} mode at 141 cm^{-1} and B_{3u} mode at 91 cm^{-1} are connected with the rotation of the chains around the b -axis.

The following modes involve mainly the displacements of Na atoms: $225 \text{ cm}^{-1} (B_{2u})$, $251 \text{ cm}^{-1} (B_{3u})$, $181 \text{ cm}^{-1} (B_{1u})$.

C. Spectra of electron excitations

With obtained values of the effective charges, we estimated the crystal field energies of the $3d$ electron localized at the V^{4+} ion site. The crystal field parameters $B_2^0 = 1360 + 2090G$, $B_2^1 = 2020 - 1590G$, $B_2^2 = 820 + 640G$, $B_4^0 = 610 + 1430G$, $B_4^1 = -1810 - 3690G$, $B_4^2 = 33 + 144G$, $B_4^3 = 3650 + 8180G$, $B_4^4 = 4070 + 7420G \text{ cm}^{-1}$ for the V_1 , V_3 sites were calculated in the framework of the exchange charge model [27] (for the V_2 , V_4 sites B_p^1 and B_p^3 parameters change signs, the first terms correspond to point charge contributions, the Stevens normalization is used). The scaling factor G determines the strength of the exchange charge field. We estimated this phenomenological parameter of the model ($G = 4$) by fitting the total crystal field splitting to the width of the V– $3d$ bands presented in Ref. [13]. In this case, the effective crystal field provides the following energy level pattern of the V^{4+} ion : $0 (A'')$, $1.10 (A')$, $1.18 (A'')$, $3.39 (A')$ and $4.78 (A')$ eV (irreducible representations of the C_s point group, corresponding to the space symmetry of the electron wave function, are given in brackets, additional shifts of the crystal field levels due to the spin-orbit interaction and the electrostatic field of a hole at the neighboring vanadium site are less than 0.025 eV). The ground state wave function is the d_{xy} orbital with small admixture of the d_{yz} orbital as it has been already pointed earlier [13], and the sequence of the excited states is in agreement with results of the band structure calculations as well [13].

The strong absorption of light ($\mathbf{k}||\mathbf{c}$) with the $\mathbf{E}||\mathbf{a}$ as well as with $\mathbf{E}||\mathbf{b}$ polarizations was observed in the region of $1.0\text{--}1.2 \text{ eV}$ [21]. Both magnetic dipole and induced electric dipole $d-d$ transitions in the odd crystal field are allowed between the A'' states for $\mathbf{E}||\mathbf{a}$, and between the A'' and A' states for $\mathbf{E}||\mathbf{b}$. Thus, in accordance with the results on the crystal field energies given above, the observed broad optical bands in the region of 1 eV can be interpreted as phonon assisted $d-d$ transitions without any additional suppositions about the broken symmetry between legs of vanadium ladders [28].

The next step towards the detailed description of the spectra of electron excitations is to construct molecular orbitals for the $[\text{V}_2\text{O}]^{7+}$ “molecule” having C_{2v} point symmetry, from the vanadium d -orbitals and oxygen p -orbitals. The vanadium ground state wave function d_{xy} yields the non-bonding a_2 orbital as well as bonding and antibonding b_2 molecular orbitals, namely,

$$\begin{aligned} a_2 &: [d_{xy}(L) + d_{xy}(R)] \\ b_2 &: [d_{xy}(L) - d_{xy}(R)] + p_y \\ b_2^* &: [d_{xy}(L) - d_{xy}(R)] - p_y. \end{aligned}$$

Here, a_2 , b_2 denote irreducible representations of the C_{2v} point group, the asterisk refers to an antibonding orbital, L and R stand for the vanadium sites at the left and, correspondingly, right sides of a ladder rung. The highest

filled orbital being a_2 , the $a_2 \rightarrow b_2^*$ electronic transition allowed in $\mathbf{E}||\mathbf{a}$ polarization could account for the low-frequency absorption band observed just in this polarization. Quantum-chemical calculations are necessary to verify this qualitative interpretation.

D. Fano resonances with a continuum

The asymmetric lineshapes of the infrared active modes at 91, 150, 939 cm^{-1} in $\mathbf{E}||\mathbf{a}$ polarization bring into evidence a strong interference between these modes and a continuum observed just in this polarization. This interpretation is supported by the fact that the spectral line near 91 cm^{-1} becomes perfectly symmetric when the continuum absorption vanishes in this spectral range below the phase transition temperature $T_c = 35$ K. In our earlier work [8] we argued that these changes are connected with the opening of a gap in the magnetic excitation spectrum at T_c , the observed continuum being due to two-magnon absorption.

However, such a straightforward interpretation is no more valid in the case of the space group D_{2h}^{13} . It should be revised, taking into account possible electronic excitations in this frequency range, as discussed in the previous section, and a charge ordering at the transition temperature.

E. Higher order infrared vibrational spectra

Two- and three-phonon absorption occurs due to anharmonicity of crystal vibrations. It is continuous, displaying singularities corresponding to critical points of the Brillouin zone. Leaving the detailed analysis of multiphonon bands to a future publication, we discuss here only sharp lines observed in $\mathbf{E}||\mathbf{c}$ absorbance spectrum (Fig. 5). They are listed in Table 5 together with their tentative assignment, using symmetry allowed combinations of Γ -point phonons observed in our first-order spectra. The coincidence of the observed and combinational frequencies is within the precision of our measurements.

The strongest narrow peak at 1930 cm^{-1} corresponds, according to this assignment, to a sum of the components of the Davydov doublet originating from the V–O3 stretching vibration. This stretching mode is well localized which results in its small dispersion over the Brillouin zone, thus delivering a narrow two-phonon band, in accordance with the experimental observation.

V. SUMMARY

We have performed a thorough spectroscopic study of far infrared reflection and transmission as well as Raman scattering of α' - NaV_2O_5 single crystals in the high temperature phase (above $T_c = 35$ K). Far infrared spectra were obtained for $\mathbf{E}||\mathbf{a}$, $\mathbf{E}||\mathbf{b}$ and $\mathbf{E}||\mathbf{c}$ polarizations of incident light. Diagonal (aa), (bb), (cc) as well as nondiagonal (ab), (bc), (ac) components of the Raman scattering tensor were investigated. We report five infrared active modes in $\mathbf{E}||\mathbf{a}$ polarization, four — in $\mathbf{E}||\mathbf{b}$ polarization and six — in $\mathbf{E}||\mathbf{c}$ polarization. Eight Raman active modes have been detected for parallel polarizations of incident and scattered light (aa), (bb), (cc). The (ab), (ac) and (bc) Raman geometries delivered three, seven and, correspondingly, five modes. These results are in a much better agreement with the recently proposed centrosymmetric space group D_{2h}^{13} ($Pm\bar{m}n$) for the high-temperature phase of NaV_2O_5 than with earlier accepted noncentrosymmetric space group C_{2v}^7 ($Pmn2_1$). We have also performed the lattice dynamics calculations, in the framework of the rigid ion model, for both proposed in the literature structures of NaV_2O_5 . We failed to obtain any physically well-grounded set of parameters providing a stable C_{2v}^7 lattice structure. Thus, our infrared and Raman experimental data, as well as the results of lattice dynamics calculations support strongly the conclusion of the previous structural study [13,14] that the space group of NaV_2O_5 above $T_c = 35$ K is the centrosymmetric D_{2h}^{13} rather than noncentrosymmetric C_{2v}^7 group.

This conclusion leads to important physical consequences. In particular, it requires to revise the interpretation of one-dimensional magnetic properties of NaV_2O_5 and of the phase transition at 35 K considered earlier as an ordinary spin-Peierls transition. An interpretation of the earlier observed broad bands in the near and far infrared absorption [21,8] needs to be reconsidered too.

Using the values of effective charges obtained in the process of lattice dynamics calculations and fitting the total crystal field splitting to the width of the V–3d bands [12], we estimated the crystal field energies of the 3d electron localized at the vanadium site. It follows from this estimate that the observed near infrared broad band absorption of NaV_2O_5 [21] can be interpreted as phonon assisted $d - d$ transitions. We speculate that the far infrared $\mathbf{E}||\mathbf{a}$

polarized absorption continuum might be associated with electron excitations of $[V_2O]^{7+}$ rungs in the crystal field of C_{2v} symmetry.

Strongly asymmetric spectral lines observed in $\mathbf{E}||\mathbf{a}$ absorbance spectra of NaV_2O_5 bring into evidence a strong interference between relatively narrow phonon lines and the underlying continuum. This points to an interaction between crystal vibrations and magnetic or electronic excitations. The detailed physical interpretation of the observed phenomenon depends on the nature of the far infrared $\mathbf{E}||\mathbf{a}$ polarized continuum which requires a special investigation.

In conclusion, we reported also some preliminary results on higher order vibrational spectra of NaV_2O_5 appearing due to anharmonicity of lattice vibrations.

ACKNOWLEDGMENTS

We are grateful to A. I. Smirnov for checking the samples by ESR measurements. We acknowledge A. N. Vasil'ev for stimulating discussions and G. N. Zhizhin for a constant support of this research. This work was made possible in part by the Grant No. 98-02-17620 from the Russian Fund for Basic Research.

-
- [1] M. Isobe and Y. Ueda, *J. Phys. Soc. Jap.* **65**, 1178 (1996).
 - [2] A.I. Buzdin and L.N. Bulaevskii, *Usp. Fiz. Nauk* **131**, 495 (1980) [*Sov. Phys. Usp.* **23**, 409 (1980)].
 - [3] J. Hemberger, M. Lohmann, N. Nickloas, A. Loidl, M. Klemm, G. Obermeier, and S. Horn, *Europhys. Lett.* **42**, 661 (1998); T. Yamada, private communication.
 - [4] K. Kobayashi, T. Mizokawa, A. Fujimori, M. Isobe, and Y. Ueda, *Phys. Rev. Lett.* **80**, 3121 (1998).
 - [5] Y. Fujii, H. Nakao, T. Yoshihama et al., *J. Phys. Soc. Jap.* **66**, 326 (1997).
 - [6] M. Weiden, R. Hauptmann, C. Geibel, F. Steglich, M. Fisher, P. Lemmens, and G. Guntherodt, *Z. Phys. B* **103**, 1 (1997).
 - [7] H. Curoe, H. Seto, J. Sasaki, T. Sekine, M. Isobe, and Y. Ueda, *J. Phys. Soc. Japan*, in press, cond-mat/9805251.
 - [8] M.N. Popova, A.B. Sushkov, A.N. Vasil'ev, M. Isobe, and Y. Ueda, *Pis'ma v ZhETF* **65** 711 (1997) [*JETP Lett.* **65** 743 (1997)], cond-mat/9711052.
 - [9] D. Smirnov, P. Millet, J. Leotin, D. Poilblanc, J. Riera, D. Augier, and P. Hansen, *Phys. Rev. B* **57**, R11035 (1998).
 - [10] T. Yoshihama, M. Nishi, K. Nakajima, Y. Fujii, M. Isobe, and Y. Ueda, *Physica B* **234-236**, 539 (1997).
 - [11] A. Carpy and J. Galy, *Acta Crystallogr. B* **31**, 1481 (1975).
 - [12] H.G. Backman, F.R. Ahmed, and W.H. Barnes, *Z. Krist.* **115**, 110 (1961).
 - [13] H. Smolinski, C. Gros, W. Weber, U. Peuchert, G. Roth, M. Weiden, and C. Geibel, *Phys. Rev. Lett.* **80**, 5164 (1998).
 - [14] A. Meetsma, J.L. de Boer, A. Damascelli, T.T.M. Palstra, J. Jegoudez, and A. Revcolevschi, *Acta Cryst.*, in press, cond-mat/9806081.
 - [15] P. Horsch and F. Mack, cond-mat/9801316.
 - [16] T. Ohama, H. Yasuoka, M. Isobe, and Y. Ueda, preprint.
 - [17] H. Seo and H. Fukuyama, cond-mat/9805185.
 - [18] M.V. Mostovoy and D.I. Khomskii, cond-mat/9806215.
 - [19] P. Thalmeier and P. Fulde, cond-mat/9805230.
 - [20] M. Köppen, D. Pankert, R. Hauptmann, M. Lang, M. Weiden, C. Geibel, and F. Steglich, *Phys. Rev. B* **57**, 8466 (1998).
 - [21] S.A. Golubchik, M. Isobe, A.N. Ivlev, B.N. Mavrin, M.N. Popova, A.B. Sushkov, Y. Ueda, and A.N. Vasil'ev, *J. Phys. Soc. Japan* **66**, 4042 (1997).
 - [22] L. Abello, E. Husson, Y. Repelin, and G. Lucazeau, *Spectrochimica Acta* **39A**, 641 (1983).
 - [23] M. Isobe, C. Kagami, and Y. Ueda, *J. Crystal Growth* **181**, 314 (1997).
 - [24] B.N. Mavrin, *Optika i Spectroscopiya* **49**, 79 (1980).
 - [25] D.L. Rousseau, R.P. Bauman, and S.P.S. Porto, *J. Raman Spectr.* **10**, 253 (1981).
 - [26] U. Fano, *Phys. Rev.* **124**, 1866 (1961).
 - [27] B.Z. Malkin, in: *Spectroscopy of solids containing rare-earth ions*, ed. A.A. Kaplyanskii and R.M. Macfarlane, Elsevier Science PB, Amsterdam, 1987, 13-49.
 - [28] A. Damascelli, D. van der Marel, J. Jegoudez, G. Dhahenne, and A. Revcolevschi, cond-mat/9806222.

FIGURE CAPTIONS

FIG. 1. The structure of NaV_2O_5 . (a) A stereometric projection. Oxygen and vanadium atoms are at the corners of and, correspondingly, inside the pyramids. Sodium atoms are presented as balls. (b) ab projection. Apical oxygen O3 atoms (situated above or below the corresponding V atoms) are not shown. A dashed line indicates the longest V–O2 bond (0.199 nm). ab -projection of the crystal unit cell is shown by a thin solid line.

FIG. 2. Room temperature far-infrared reflectivity spectra of NaV_2O_5 . Open circles represent experimental data. Solid lines are the result of the fitting (see the text).

FIG. 3. Absorption coefficient α in the region of low frequency absorption bands at room temperature. An arrow indicates a Fano-type resonance. It is shown separately in the inset. Open circles represent experimental data. Solid line in the main figure was calculated using the parameters obtained from the fitting of the reflectance spectrum. Solid line in the inset is a result of the fitting by the expression (5) with $\alpha_B(\omega)$ shown as a dashed line.

FIG. 4. Fano resonance near 91 cm^{-1} at the temperature of 40 K (open circles) and its fitting by the equation (5) with parameters $\omega_r = 90.7 \text{ cm}^{-1}$, $\gamma = 0.2 \text{ cm}^{-1}$, $q = -1.0$, $\alpha_B(\omega_2) = 270 \text{ cm}^{-1}$, $\alpha_0/\alpha_B = 0.3$ (solid line). The temperature dependence of the Fano parameter q is given in the left inset. The right inset presents the absorption spectrum in the vicinity of 91 cm^{-1} line at 6 K taken with the resolution of 0.05 cm^{-1} (open circles) and its fitting by the Lorentzian with a FWHM= 0.10 cm^{-1} .

FIG. 5. Absorbance spectrum of NaV_2O_5 in the region of multiphonon bands at room temperature.

FIG. 6. Room temperature Raman spectra of NaV_2O_5 . Asterisks mark A_g lines seen in B_{ig} ($i = 1, 2, 3$) spectra.

FIG. 7. Room temperature Raman spectra of $\text{Na}_{1-x}\text{V}_2\text{O}_5$ for different x .

FIG. 8. Decomposition of the room temperature $c(aa)\bar{c}$ Raman spectrum of NaV_2O_5 into separate contours (dashed lines). The sum of these contours shown by a solid line approximates the experimental spectrum (circles) rather well.

TABLE I. Infrared active vibrational modes and dielectric constants of NaV₂O₅ (all frequencies are in cm⁻¹)

Polarization, mode symmetry	Observed													Calculated (<i>Pmmn</i>)	
	Transmission						Reflection							ω_{TO}	ω_{LO}
	$T = 40$ K			$T = 300$ K			$T = 300$ K				$f \cdot 10^3$	ϵ_∞	ϵ_0		
ω_{TO}	γ_{TO}	ω_{TO}	γ_{TO}	$\epsilon_{\omega_1}^a$	$\epsilon_{\omega_2}^a$	ω_{TO}	γ_{TO}	ω_{LO}	γ_{LO}	ϵ_∞				ϵ_0	ω_{TO}
E c					7.5	7.5	162	5.2	165	5.7	45	3.9	7.7	216	219
<i>B_{1u}</i> (<i>Pmmn</i>)					± 0.2	± 0.2	179	8.4	212	8.3	130			232	256
or							—							298	298
<i>B₂</i> (<i>Pmn2₁</i>)							468	38.0	483	38.0	23			430	430
							591	119.9	594	119.0	6.8			589	690
							760	59.4	762	59.3	1.6			691	716
							955	2.5	1017	3.0	39			961	1036
E b	178	4	175	12	5.2	10.2	175	8.3	180	8.4	39	4.9	9.5	141	173
<i>B_{2u}</i> (<i>Pmmn</i>)	225	1	—		± 0.2	± 0.2								240	266
or	371		367	16			365	12.8	378	13.3	60			388	483
<i>B₁</i> (<i>Pmn2₁</i>)	594	13	582				584	29.5	769	29.0	271			578	747
E a	91 ^c		—		9.6	15.0						7.7	15.8	111	126
<i>B_{3u}</i> (<i>Pmmn</i>)	140 ^b		145 ^b		± 0.3	± 0.6	153	33.0	154	34.1	46			130	177
or	254		251				251	7.3	252	8.2	9			227	276
<i>A₁</i> (<i>Pmn2₁</i>)	—		—				—							493	534
	531	18	526	53			525	39.5	621	52.4	208			538	653
	—		—				—							742	808
			939 ^d											955	957

^a $\omega_1 = 3200$ cm⁻¹, $\omega_2 = 40$ cm⁻¹.

^bAsymmetric line.

^cFano-type resonance: $\omega_r = 90.7$ cm⁻¹, $\gamma = 0.2$ cm⁻¹, $q = -1.0$, $\alpha_0/\alpha_B = 0.3$.

^dFano-type resonance: $\omega_r = 939$ cm⁻¹, $\gamma = 1.0$ cm⁻¹, $q = 1.1$, $\alpha_0/\alpha_B = 0.2$.

 TABLE II. Room temperature Raman frequencies (cm⁻¹) for NaV₂O₅

<i>aa, bb, cc</i>	<i>ab</i>		<i>ac</i>		<i>bc</i>	
<i>A_{1g}</i> (<i>Pmmn</i>) or <i>A₁</i> (<i>Pmn2₁</i>)	Observed	Calc.(<i>Pmmn</i>)	Observed	Calc.(<i>Pmmn</i>)	Observed	Calc.(<i>Pmmn</i>)
90 (<i>cc, aa</i>)	91		174	191	141	129
177 (<i>aa, bb, cc</i>)	226		295	288	186	193
233 (<i>bb</i>)	319		683	679	225	296
301 (<i>aa, bb</i>)	362				392	332
420 (<i>bb, cc</i>)	439				429	410
447 (<i>aa</i>)	518				550	619
533 (<i>aa, bb</i>)	626				—	798
970 (<i>cc, aa</i>)	964				951	961

TABLE III. Comparison of experimentally observed Raman and infrared modes with the expected ones within centrosymmetric D_{2h}^{13} and noncentrosymmetric C_{2v}^7 space groups (mode frequencies are in cm^{-1})

$Pm\bar{m}n(D_{2h}^{13})$		Observed modes								$Pmn2_1(C_{2v}^7)$
$8A_g(aa, bb, cc)$	90	177	233	301	420	447	533	970	\	$15A_1(aa, bb, cc; \mathbf{E} \mathbf{a})$
$7B_{3u}(\mathbf{E} \mathbf{a})$	91 ^a	145	251	526	939				/	
$3B_{1g}(ab)$	174	295	683						\	$7B_1(ab; \mathbf{E} \mathbf{b})$
$4B_{2u}(\mathbf{E} \mathbf{b})$	175	225 ^a	367	582					/	
$8B_{2g}(ac)$	141	186	225	392	429	550	951		\	$15B_2(ac; \mathbf{E} \mathbf{c})$
$7B_{1u}(\mathbf{E} \mathbf{c})$	162	179	468	591	760	955			/	
$5B_{3g}(bc)$	169	257	366	418	683				\	$8A_2(bc)$
$3A_u$									/	

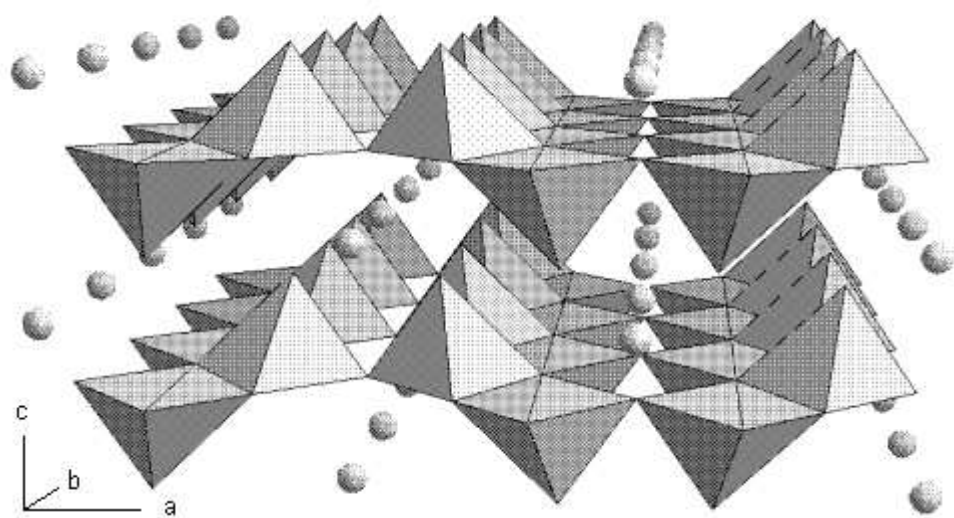
^aObserved below 200 K.

TABLE IV. The bond lengths (nm) in NaV_2O_5 and V_2O_5

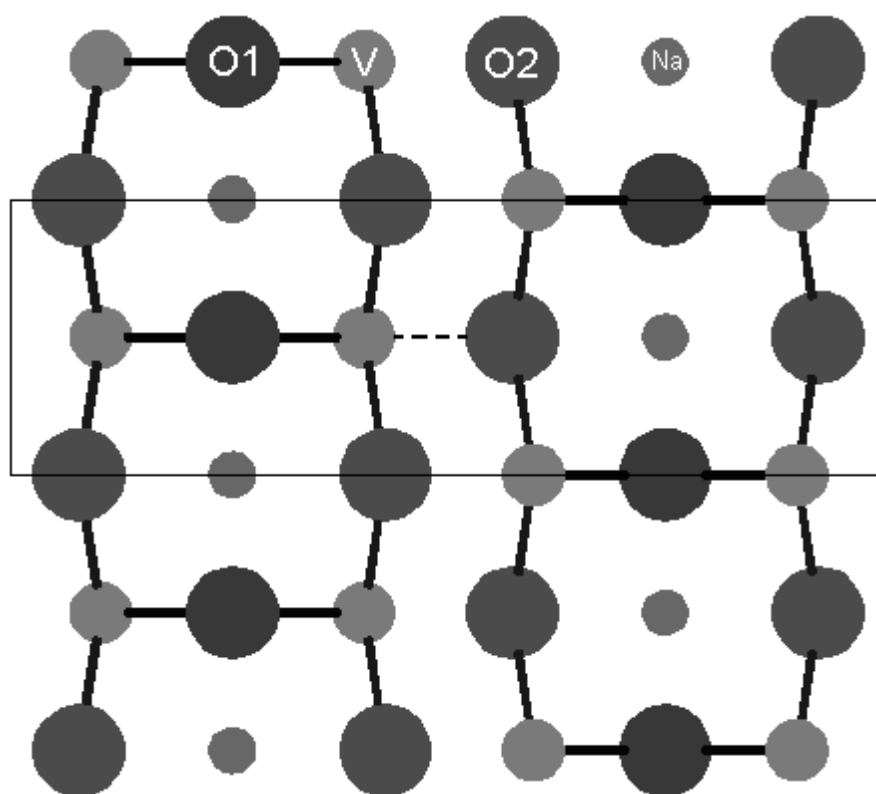
Bond	NaV_2O_5 [13]	V_2O_5 [22]
V–O3	0.161	0.158
V–O1	0.183	0.177
(V–O2)×2	0.192	0.188
V–O2′	0.199	0.202
V–O3′	0.318	0.278

TABLE V. Multiphonon bands in NaV_2O_5 observed in $\mathbf{E}||\mathbf{c}$ polarization

Observed bands, cm^{-1}	Combination of phonons, cm^{-1}		
1072 (B_{1u})	550 (B_{2g})	+ 526 (B_{3u})	= 1076 (B_{1u})
1270 (B_{1u})	683 (B_{3g})	+ 582 (B_{2u})	= 1265 (B_{1u})
1930 (B_{1u})	970 (A_g)	+ 955 (B_{1u})	= 1925 (B_{1u})
2858 (B_{1u})	3 × 955 (B_{1u})		= 2865 (B_{1u})
2901 (B_{1u})	2 × 970 (A_g)	+ 955 (B_{1u})	= 2895 (B_{1u})



(a)



(b)

